POLITECNICO
MILANO 1863

SCUOLA DI INGEGNERIA INDUSTRIALE
E DELL'INFORMAZIONE

Advanced Dynamics of Mechanical Systems

Assignment 1: modal analysis of a cantilever beam and a light rail wheel

Authors:

Barutta E.	10726132
Meneghini D.	10715030
Milic K.	11012938
Visentin N.	10797203

Lecturers:
Melzi S.
Pomaranzi G.

Academic Year: 2023/24

Contents

1 Introduction

The subject of this assignment is the experimental modal analysis, with the aim of extracting modal parameters and modeshapes out of experimental data for two structures. The first structure is a very simple clamped beam, so an analytical study is also included: this allows to generate mathematically the "experimental" data and also allows for a comparison with the numerical results. The second structure is a rail wheel: here real data are used for the analysis.
Modal analysis is a very powerful approach, that allows to easily study a structure in a certain frequency range of interest by using just few degrees of freedom, but still offering a good approximation of its behavior in that frequency range.
Matlab was used for the implementation and all the computations.

2 Cantilever beam

2.1 Formulation of the problem

The first part of the assignment concerns the study of a an aluminium cantilever beam with rectangular section, as shown in *figure 1.* Data are provided in *table 1.*

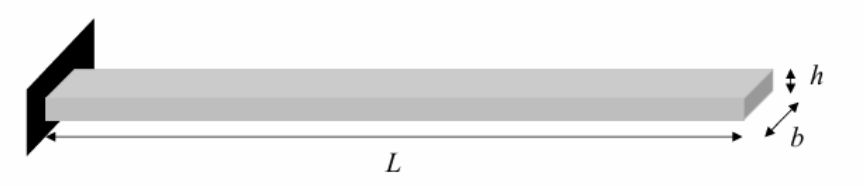

Figure 1: Cantilever beam

First, we studied the structure analytically, using the standing wave solution for the bending vibrations on a beam, in order to compute the natural frequencies and the modeshapes. Also, we computed some frequency response functions (FRFs) between assigned input and output positions: these FRFs were treated afterwards as "ficticious" experimental data, and they were used to reconstruct back numerically the FRFs and the modeshapes through an estimation algorithm (based on the FRF-based multi-mode curve fitting method).

	Symbol	**Value**	**Unit**
Beam length	L	1200	mm
Section thickness	h	8	mm
Section width	b	40	mm
Density	ρ	2700	$\frac{kg}{m^3}$
Young's modulus	E	68000	MPa

Table 1: Data of the cantilever beam

It was possible, in this way, to compare the analytical and the numerical results, in order to check the quality of the identification of the modal parameters and of the modeshapes.

2.2 Analytical study

To carry on the analytical study, we considered the model of a thin beam $(h/L = 0.0067 \ll 1)$, with a linear behaviour and homogeneous properties. The standing wave solution, in this case, is given by:

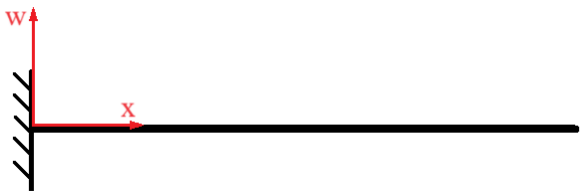

Figure 2: Model of the beam and reference system

$$w(x,t) = [Acos(\gamma x) + Bsin(\gamma x) + Ccosh(\gamma x) + Dsinh(\gamma x)] \cdot cos(\omega t + \varphi) \quad , \quad \textit{where } \gamma = \sqrt[4]{\frac{m\omega^2}{EJ}} \textit{ and } \omega = 2\pi f \tag{1}$$

Being:

- $w(x,t)$ the vertical displacement of the beam as a function of x (see *figure 2*) and time
- A, B, C, D unknown coefficients
- m, E, J properties of the beam (see *table 1*)
- f, ω, φ the vibration frequency, pulsation and phase

Modeshapes Equation (1) has two terms: one is a function of space and the second one depends on time. The four unknowns of the spatial term (modeshapes) are computed by applying the boundary conditions:

$$\begin{cases} w(0,t) = 0, \ \forall t \quad \rightarrow \quad \textit{no displacement at } x = 0 \\ w'(0,t) = 0, \ \forall t \quad \rightarrow \quad \textit{no rotation at } x = 0 \\ EJw'''(L,t) = 0, \ \forall t \quad \rightarrow \quad \textit{no shear action at } x = L \\ EJw''(L,t) = 0, \ \forall t \quad \rightarrow \quad \textit{no moment at } x = L \end{cases}$$

After computing the derivatives and applying these conditions the system becomes, in matrix form:

$$[H(\omega)] \cdot \underline{X} = \underline{0} \quad , \quad \textit{where } \underline{X} = \begin{bmatrix} A & B & C & D \end{bmatrix}^T \textit{ and } [H(\omega)] \textit{ is the matrix of coefficients of the system} \tag{2}$$

In particular $[H(w)]$ results to be:

$$[H(\omega)] = \begin{bmatrix} 1 & 0 & 1 & 0 \\ 0 & \gamma & 0 & \gamma \\ sin(\gamma L) & -cos(\gamma L) & sinh(\gamma L) & cosh(\gamma L) \\ -cos(\gamma L) & -sin(\gamma L) & cosh(\gamma L) & sinh(\gamma L) \end{bmatrix} \quad , \quad \textit{remember that } \gamma = \sqrt[4]{\frac{m\omega^2}{EJ}}$$

In order to find the non trivial solutions we need to solve $det[H(\omega)] = 0$, where the solutions are the natural frequencies of the system. Of course we will have an infinite number of them, because the beam is a continuous body, but we will limit our study to the frequency range from 0 to 200 Hz. In this range there are four natural frequencies, which are shown in *figure 3*:

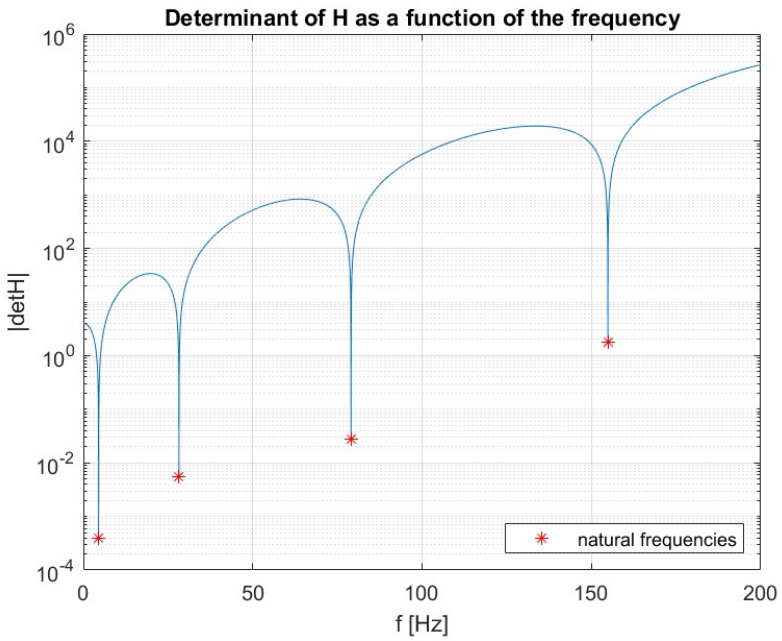

Figure 3: First four natural frequencies of the beam $[Hz]$*:* $f_1 = 4.5;\ f_2 = 28.2;\ f_3 = 79.0;\ f_4 = 154.9$

After we computed the natural pulsations ω_k, we substitute them into (2), one at the time, to compute the eigenshapes (i.e. coefficients A, B, C, D):

$$[H(\omega_k)] \cdot \underline{X}^{(k)} = \underline{0} \ , \quad \textit{with} \quad \underline{X}^{(k)} = \begin{bmatrix} A^{(k)} & B^{(k)} & C^{(k)} & D^{(k)} \end{bmatrix}^T$$

Since the system is undetermined (ω_k are computed such that $det[H] = 0$), we need to normalize all coefficients with respect to one of them: dividing by A, system (2) becomes, for the k-th mode:

$$\left[\begin{array}{c|ccc} \cdots & \cdots & \cdots & \cdots \\ \hline \underline{N}(\omega_k) & & [\hat{H}(\omega_k)] & \end{array}\right] \cdot \left[\begin{array}{c} 1 \\ \hline \underline{\hat{X}}^{(k)} \end{array}\right] = \underline{0} \ , \quad \textit{with} \quad \underline{\hat{X}}^{(k)} = \begin{bmatrix} \hat{B}^{(k)} & \hat{C}^{(k)} & \hat{D}^{(k)} \end{bmatrix}^T \textit{ and } \hat{B}^{(k)} = \frac{B^{(k)}}{A^{(k)}}, \textit{ etc}$$

We can now solve for $\underline{\hat{X}}^{(k)}$:

$$\underline{\hat{X}}^{(k)} = -\left[\hat{H}(\omega_k)\right]^{-1} \cdot \underline{N}(\omega_k) \tag{3}$$

After we have solved (3) for each natural frequency, we can compute the actual modeshapes (recall (1)), that are shown in *figure 4*:

$$\Phi_k(x) = [1 \cdot cos(\gamma_k x) + \hat{B}^{(k)} sin(\gamma_k x) + \hat{C}^{(k)} cosh(\gamma_k x) + \hat{D}^{(k)} sinh(\gamma_k x)]$$

The plots of the four modeshaphes are normalized for a better visualisation. For each modeshape the displacement at $x = 0$ is zero, which is consistent with the constraints. On the other hand, the maximum displacement occurs at the extreme point $x = L$. Notice that the numbers of nodes (point with zero displacement $\forall t$) increases with the natural frequency.

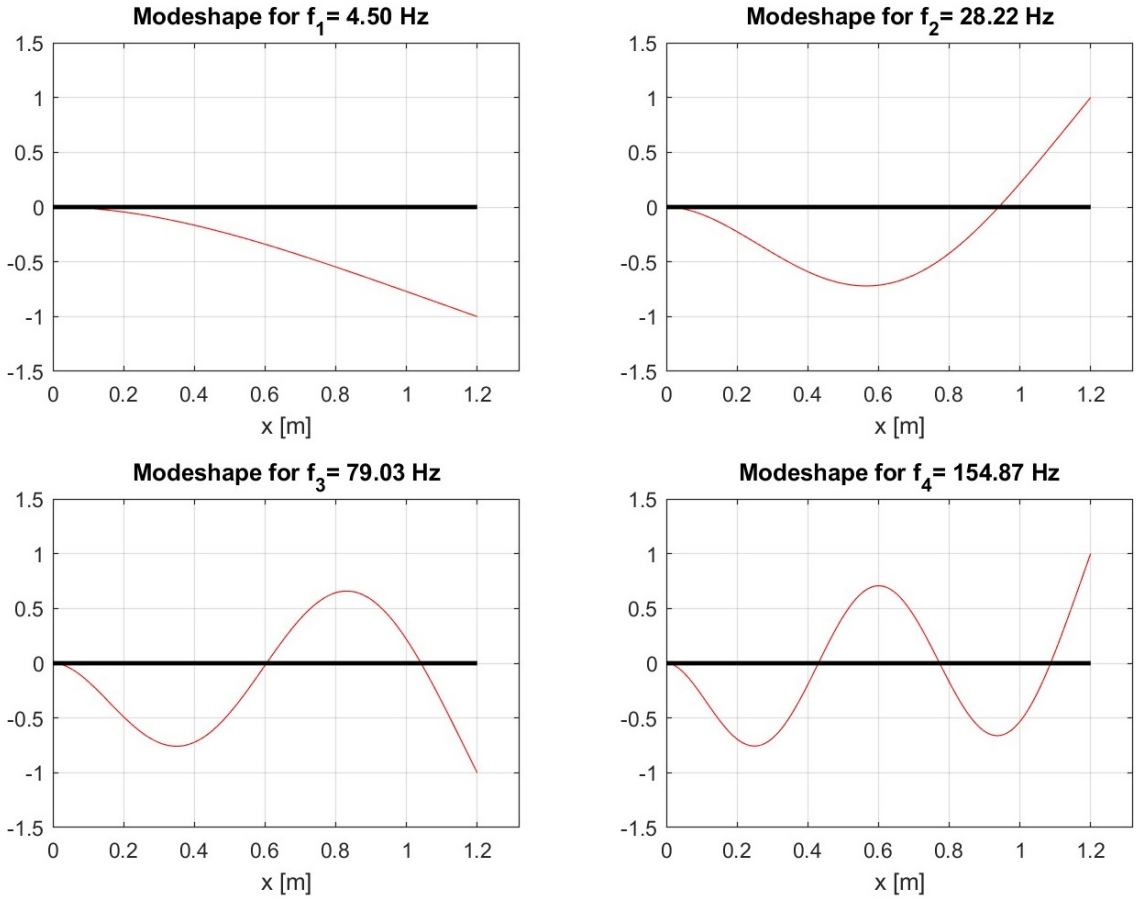

Figure 4: First four modeshapes of the beam

Frequency response functions The frequency response functions between input forces and output displacements are computed using the modal approach. In our case, we only have one harmonic force $F_m(t) = F_{m0}\, e^{j\Omega t}$ acting on the tip of the beam, however, in general, using this approach, the FRF between the $m-th$ input and the $i-th$ output (G_{im}) can be calculated as the superposition of many modal contributions, leading to:

$$G_{im}(\Omega) = \sum_{k=1}^{n} \frac{\Phi_k(x_m)\Phi_k(x_i)/m_k}{-\Omega^2 + 2j\xi_k\omega_k\Omega + \omega_k^2} \quad , \quad \textit{where } n \textit{ is the number of modes we are considering} \tag{4}$$

In order to compute the FRFs we need to choose the position of the input force denoted by x_m (we could have also taken multiple input forces) and the positions of the outputs denoted by x_i. Moreover we also have to define the nondimensional dampings ξ_k of each mode, that in this case have been chosen as $\xi_k = 0.01\ \forall k$, which is typical for aluminium structures. Finally we have to compute modal masses m_k, which are defined as:

$$m_k = \int_0^L m\ \Phi_k^2(x)\ dx$$

In our analysis we considered one input position $x_m = 1.2\ m$ (as previously mentioned) and two output positions $x_1 = 0.3\ m$ and $x_2 = 0.95\ m$, as shown in *figure 5*.

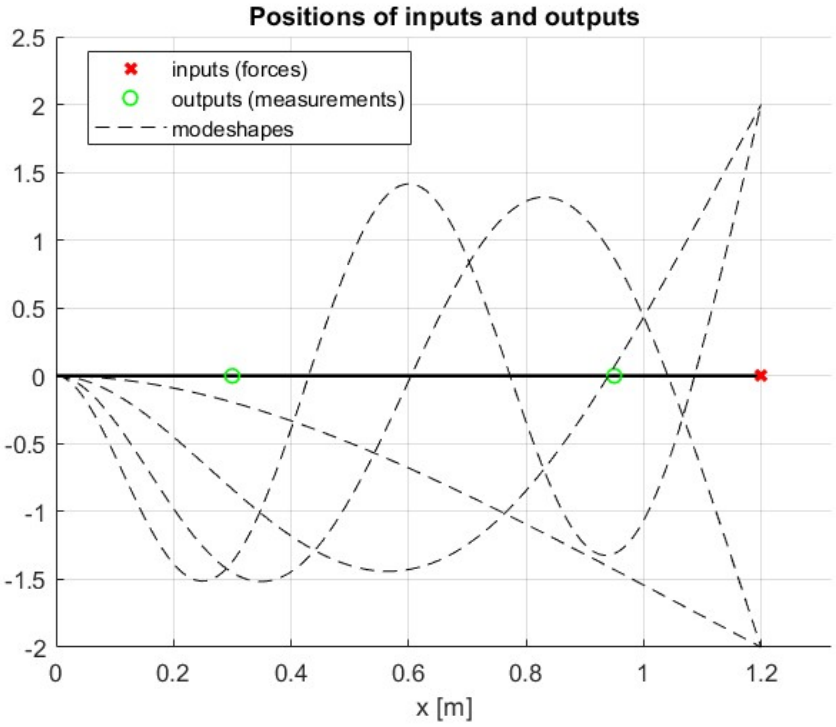

Figure 5: Input-outputs configuration on the beam

The resulting FRFs are plotted below, in terms of module and phase:

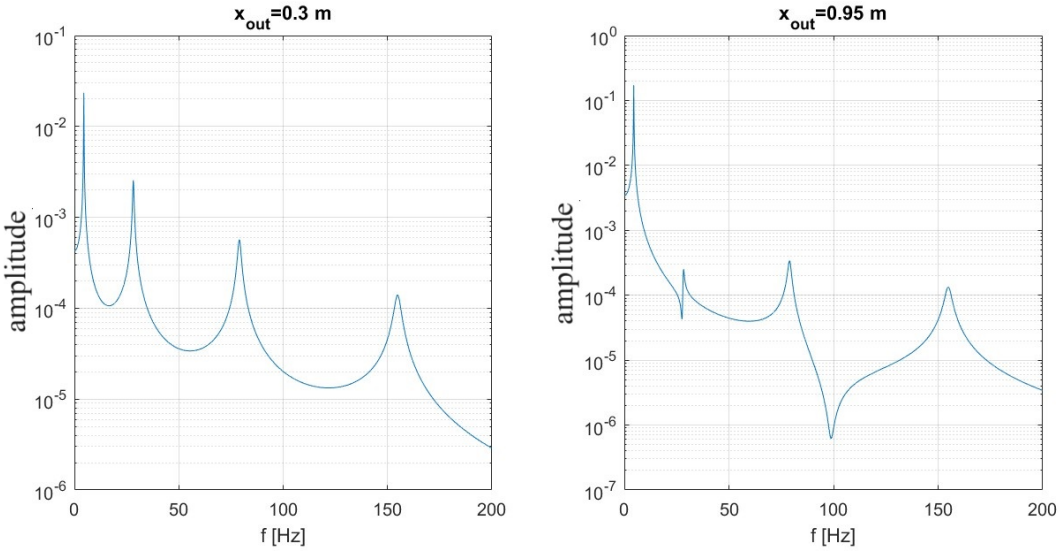

Figure 6: Amplitude of the FRFs

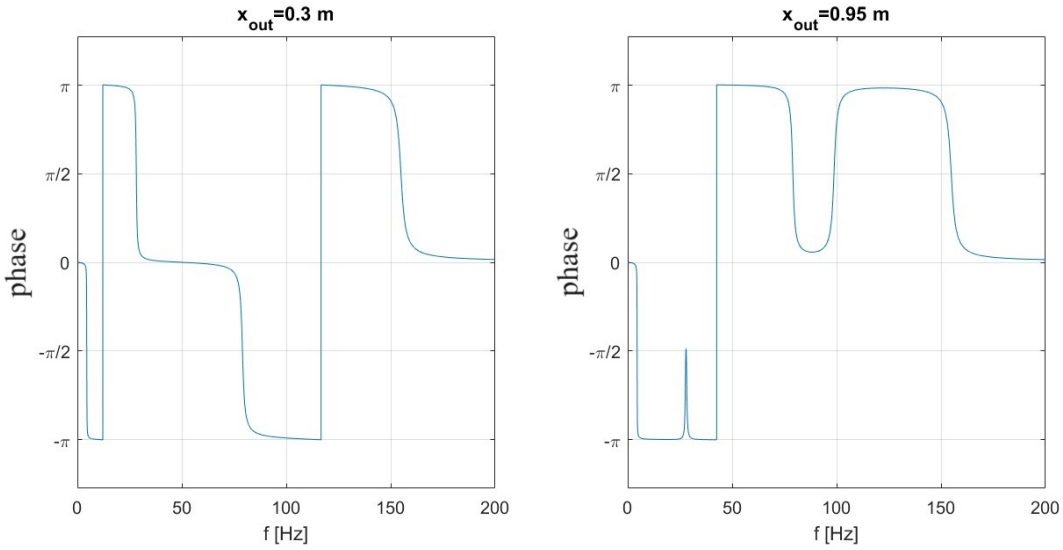

Figure 7: Phases of the FRFs

We have chosen two different output positions in order to study one case ($x_1 = 0.3\ m$) where the output is far from the nodes, and another case ($x_2 = 0.95\ m$) where it is placed next to a node of the second mode.
As we can see from *figure 6*, the FRF for x_1 shows four peaks corresponding to the resonance behaviour for each mode. On the other hand, the FRF for x_2 has three clear peaks associated to the first, third and fourth natural frequencies, but when we look at the second mode, we can't see a clear resonance. Instead, we distinguish sort of an anti resonance followed immediately after by a "small" peak.
In order to understand that, we need to consider equation 4, recalling that, if we are evaluating the FRF around $\Omega \approx \omega_k$, the contribution of k-th mode is the most relevant one. Now, it's easy to imagine that, if the sensor is placed exactly over a node, the FRF should be low and flat everywhere (numerator is zero, no displacement on a node), while if the sensor is anywhere else, at $\Omega \approx \omega_2$ we would have a peak (denominator is low, even tending to zero if damping is null). Now, since in our simulation the sensor was very close to a node of the 2^{nd} mode, we have that while approximating $\Omega = \omega_2$, both this behaviours are showing up, one immediately after the other.
Looking at *figure 7*, we can see that for x_1, at each natural frequency the phase drops by π. For x_2, at $f = f_2$, there is no phase drop, moreover there is is an increase in phase by $\pi/2$, followed by a decrease of $\pi/2$. This behaviour is again caused by the small distance between the output and the node of the second mode.

2.3 Numerical modal reconstruction

The FRFs computed in section 2.2 are now used as "fictitious" experimental data. The aim is to reconstruct modal parameters (natural frequencies, non dimensional damping ratios and modeshapes) by using a numerical approach on these data. The adopted strategy is a curve-fitting method that minimises the error, in the least squares sense, between a mathematical model for the FRF and the experimental one.

FRF reconstruction As we saw in section 2.2, equation (4) gives the analytical expression for the transfer function, taking in account for all the infinite modes. However, as we can notice from *figure 6*, the first four peaks of our FRF (the ones we are interested in) are all well separated, so we can think about reconstructing one mode at the time, separately, since the contribution for each peak is mainly covered by the resonant mode itself. The simplified model, for the *k-th* mode would be:

$$G_{im}(\Omega) \simeq \frac{\Phi_k(x_i) \cdot \Phi_k(x_m)/m_k}{-\Omega^2 + 2j\xi_k\omega_k\Omega + \omega_k^2} \tag{5}$$

$$G_{im}(\Omega) \simeq \frac{A_{im}^{(k)}}{-\Omega^2 + 2j\xi_k\omega_k\Omega + \omega_k^2} \quad , \quad \textit{calling } \Phi_k(x_i) \cdot \Phi_k(x_m)/m_k = A_{im}^{(k)} \tag{6}$$

However, to have a more refined approximation, we are also taking in account for a "simplified contribution" of the other modes, given by two residuals: one expressing the effect of the modes before the one we are studying, the other one expressing the effect of the modes after it. The expression becomes:

$$G_{im}(\Omega) \simeq \frac{A_{im}^{(k)}}{-\Omega^2 + 2j\xi_k\omega_k\Omega + \omega_k^2} + \frac{R_{im}^{(left)}}{\Omega^2} + R_{im}^{(right)} \tag{7}$$

Notice that here $A_{im}^{(k)}$ is a real number (see definition in (6)), because we assumed to have a diagonal modal damping matrix. However, this term should be a complex number, but usually its imaginary part is really small. $R_{im}^{(left)}$ and $R_{im}^{(right)}$ are, instead, complex numbers.
A graphical representation of this is given in (*figure 8*).

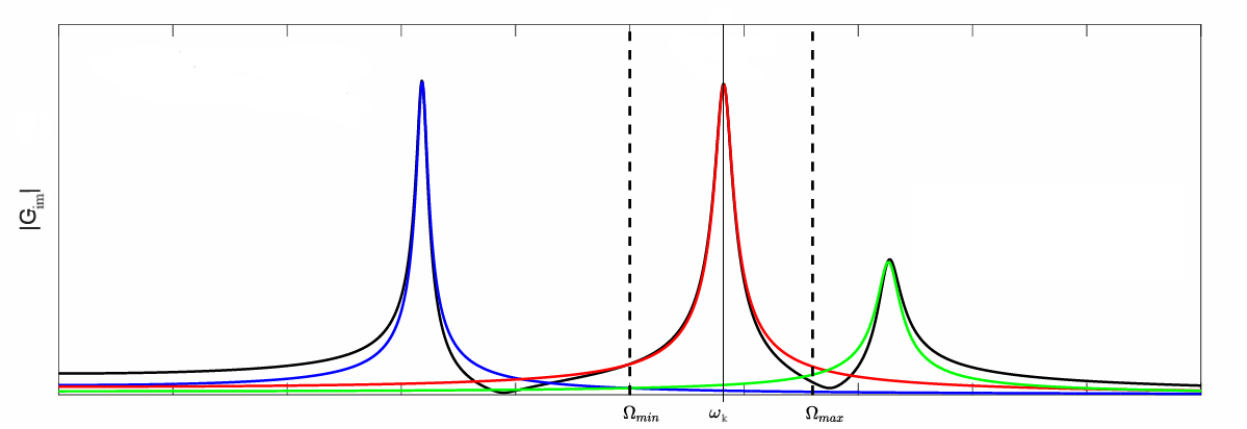

Figure 8: FRF can be seen as the superposition of many modal contributions (here the red, blue and green curves). As we can see, around a certain peak (between Ω_{min} and Ω_{max}), there is a dominant contribution given by the resonant mode

We can now compare equation (7) with the experimental data, around each natural frequency, and define an error function between the experimental and the numerical FRF, scrolling through all the M frequencies of the frequency vector:

$$\varepsilon = \sum_{r=1}^{n}\sum_{s=1}^{M}\left[Re\left(G_r^{exp}(\Omega_s) - G_r^{num}(\Omega_s)\right)^2 + Im\left(G_r^{exp}(\Omega_s) - G_r^{num}(\Omega_s)\right)^2\right]$$

Using a minimisation algorithm in Matlab, it is finally possible to compute the values of the modal parameters $\omega_k, \xi_k, A_{im}^{(k)}$ and the residuals $R_{im}^{(left)}, R_{im}^{(right)}$ that minimize the error, finding the reconstruction that best fits the experimental data.

Initial conditions for the minimization Of course, since the algorithm iterates different values of ω_k, ξ_k, $A_{im}^{(k)}$, $R_{im}^{(left)}$, $R_{im}^{(right)}$, it is required to choose some initial guesses that have to be close enough to the expected final values in order for the procedure to be effective. We used the following strategies:

- Natural frequencies: it is just sufficient to look at the FRF plot (*figure 6*) and find the frequencies where we see the peaks
- Damping coefficients: we used the phase derivative method, that allows to estimate ξ_k as:

$$\xi_k = -\frac{1}{\omega_k \cdot \frac{\partial \angle G_{im}}{\partial \Omega}\Big|_{w_k}} \quad , \quad \textit{where } \frac{\partial \angle G_{im}}{\partial \Omega}\Big|_{w_k} \textit{ is computed numerically from the phase of } G_{im}^{(exp)}$$

- $A_{im}^{(k)}$: computed from equation (6) evaluated in $\Omega = \omega_k$:

$$A_{im}^{(k)} = -2\ Im\left(G_{im}^{(exp)}(\omega_k)\right) \cdot \xi_k \cdot \omega_k^2$$

- Residuals: imposed equal to zero, as first guess

Modeshapes reconstruction Now we focus on the reconstruction of the modeshapes. Again, consider equation (5), evaluated at $\Omega = \omega_k$ and $\Phi_k(x_i),\ \Phi_k(x_m)$. After some computations, for the k-th mode we obtain:

$$G_{im}(\omega_k) = -j\frac{\Phi_k(x_i)\ \Phi_k(x_m)}{\omega_k c_k} \quad , \quad \textit{being } c_k = 2m_k\omega_k\xi_k$$
$$Im\left(G_{im}(\omega_k)\right) = -\frac{\Phi_k(x_i)\ \Phi_k(x_m)}{\omega_k c_k}$$

But the term $\frac{\Phi_k(x_m)}{\omega_k c_k}$ is always the same for all sensors, so we can just impose it equals to 1 and compute the modeshapes $\Phi_k(x_i)$ at each output position x_i by calculating $Im\left(G_{im}(\omega_k)\right)$. Of course, a normalization will be required to "correctly" displace them. Notice also that the contribute of the residuals is actually zero, because around $\Omega \approx \omega_k$ their phase is either ~ 0 or $\sim -\pi$, so their imaginary part is null.

Result of the reconstruction The output of the Matlab code is shown below. The reconstruction seems successful, both for the phase and the amplitude of the FRF (*figure 9*). Concerning the modeshapes, they are reported in *figure 10*, while a comparison between the analytical modal parameters and the reconstructed ones is shown in *table 2*.

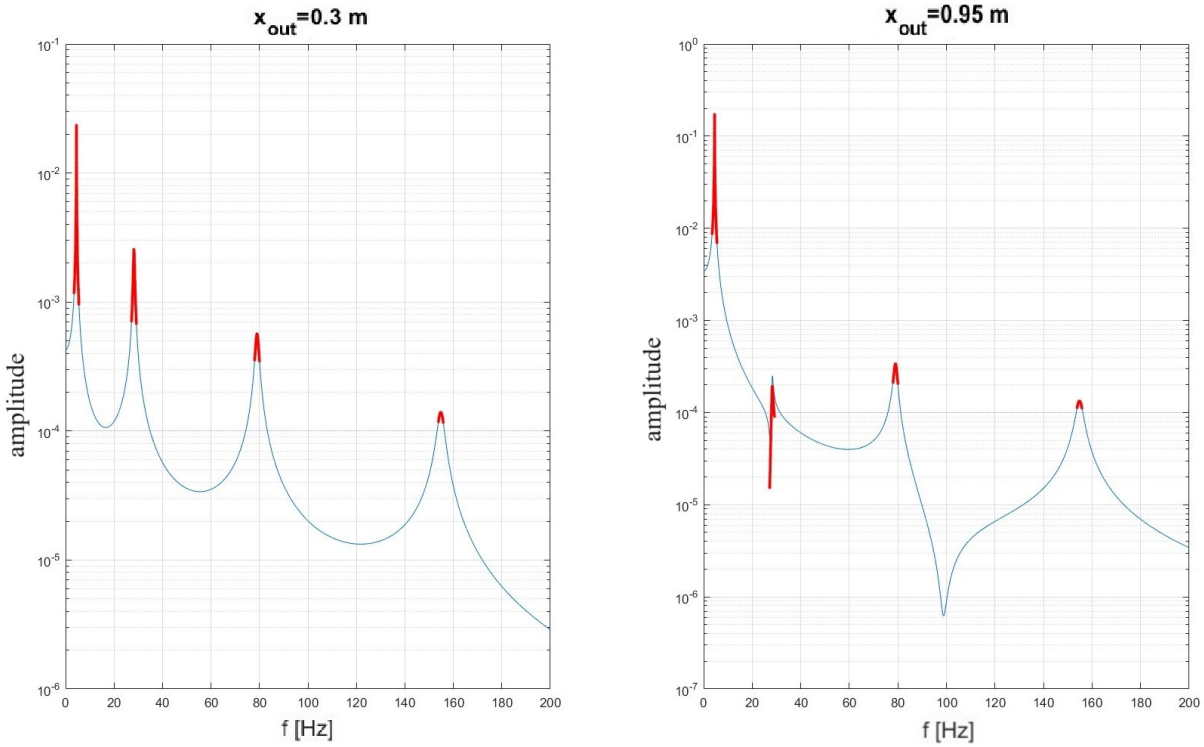

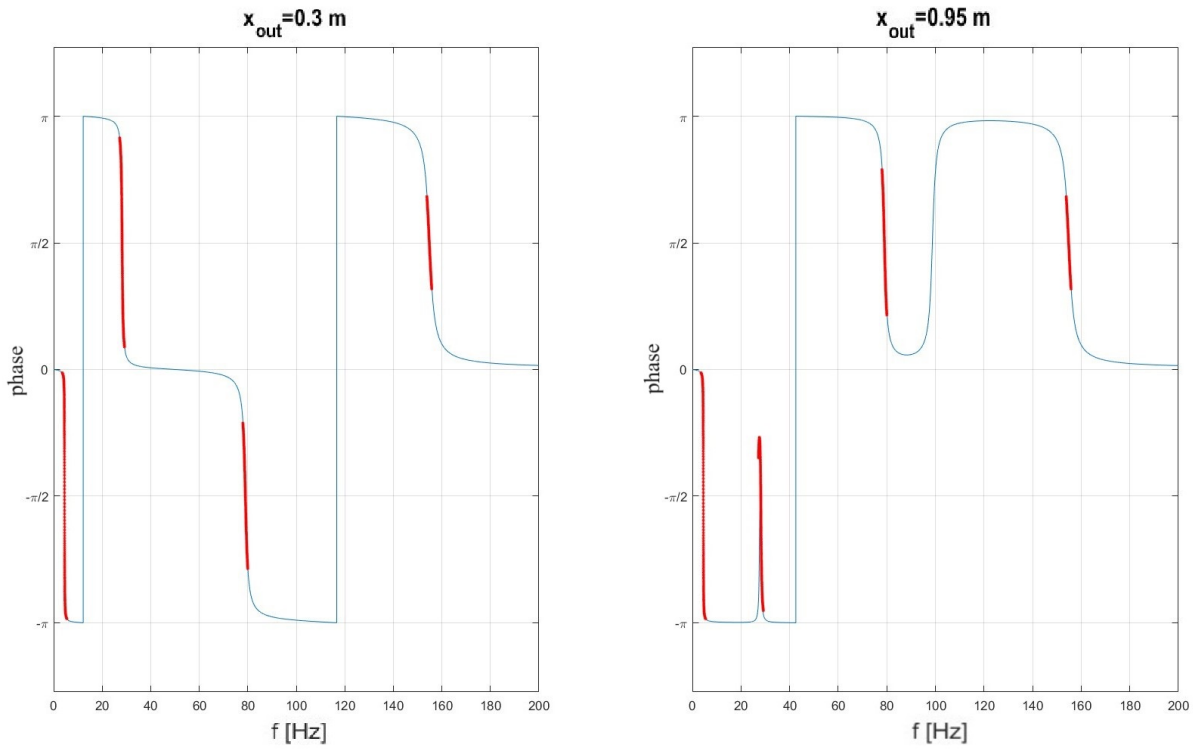

Figure 9: Reconstruction of the FRFs

Parameter	Symbol	Analytical value	Numerical value	Unit
natural frequencies	f_1	4.504	4.504	Hz
	f_2	28.224	28.220	Hz
	f_3	79.031	79.021	Hz
	f_4	154.870	154.824	Hz
nondim. dampings	ξ_1	1.00000	1.00041	%
	ξ_2	1.00000	1.00012	%
	ξ_3	1.00000	0.99974	%
	ξ_4	1.00000	1.00046	%

Table 2: Comparison between analytical and reconstructed modal parameters

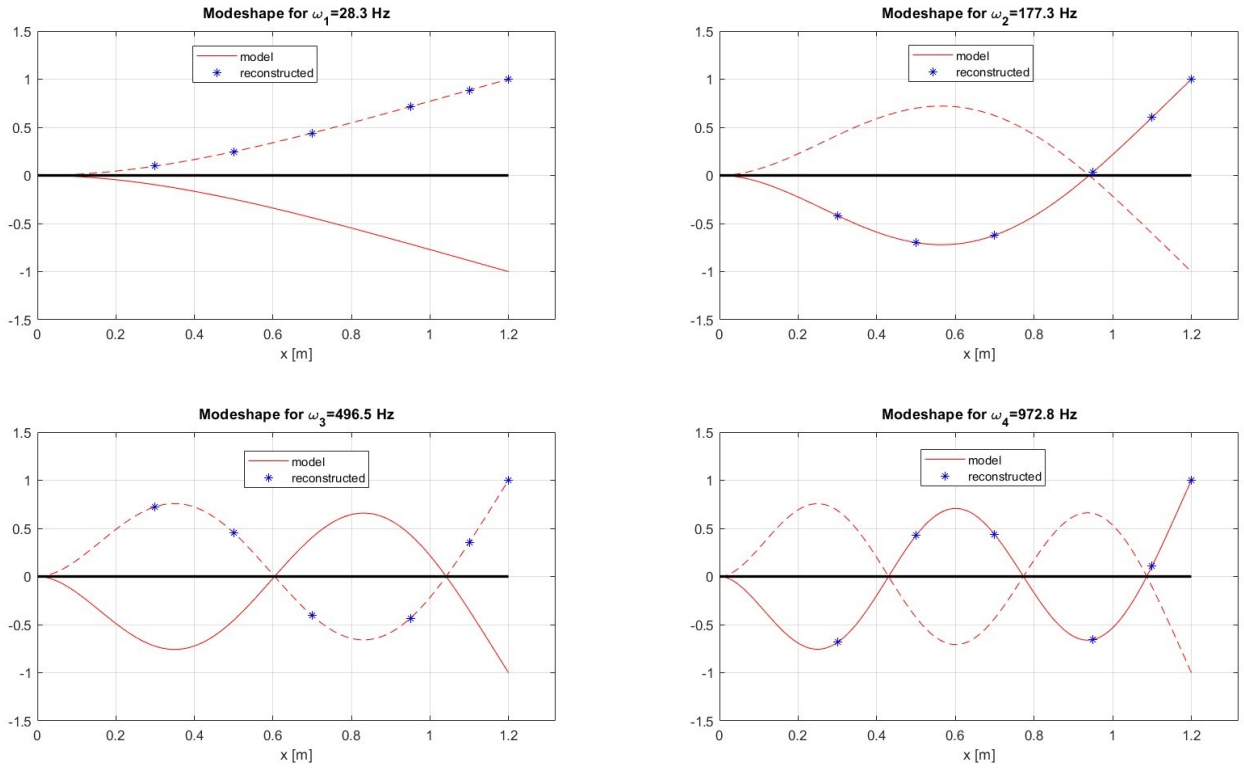

Figure 10: Reconstructed modeshapes: observe that we defined more than 2 outputs to plot this graph, to give a better idea

Notice that, when reconstructing the k-th mode, increasing the optimization frequency range too much can degrade the quality of the approximation. This occurs because in that case we are also including the influence of other modes.

3 Rail wheel

3.1 Formulation of the problem

The aim of the second part of the first assignment is to identify the modal parameters of a real system through experimental modal analysis starting from a given set of data and processing them using the single-mode identification approach developed in section 2.3. In particular, the subject of the analysis is the axial vibration of a rail vehicle wheel. This is of interest because the noise generated by these vehicles, including rolling noise and squeal noise during curves, is directly related to the vibrations of the wheel surface that produce sound.
To have a comprehensive understanding of the given data the experimental setup has to be analyzed. During operating conditions, the wheels are rigidly connected to the axle, forming the wheel-set, and rotate together with it. However, to characterize properly the wheel it's better to perform tests on the unconstrained component. This condition is called free-free condition and can be achieved by suspending the system through elastic supports (springs). It is important to note that the stiffness of these springs must be such that the corresponding "bouncing" frequency is much smaller with respect to the first natural frequency of the system. In this way, the system is not affected by the presence of the springs and can be considered as unconstrained.

Figure 11: Experimental setup

To characterize the system an impact test has been carried out. The input provided in axial direction is given through a dynamometric impact hammer, while the output is measured through piezoelectric accelerometers positioned to sense the axial vibration of the wheel rim. Twelve sensors were placed exploiting the symmetry of the structure only on half of the wheel with an angular spacing of 15°.

Figure 12: Positions of sensors and hammer impact location

The main advantage of this kind of test is the possibility to excite a very broad band of frequencies of the system but we must be aware that the analyzed data are reliable only before the maximum frequency of excitation. Then, the collected data have been processed to obtain the FRF and the coherence function. Coherence is a function defined in the frequency domain that evaluates the linear dependence between input and output signals. Its values approach one when the signals are perfectly correlated and decrease towards zero in the presence of noise, unidentified sources of excitation, or leakage effects. These data are the one we have to process so, now that we have understood the origin of the data we are able to analyze them.

3.2 Plot of the data and interpretation of the signals

The first thing to do is to plot the data and make predictions regarding the results to be expected from the subsequent analysis.

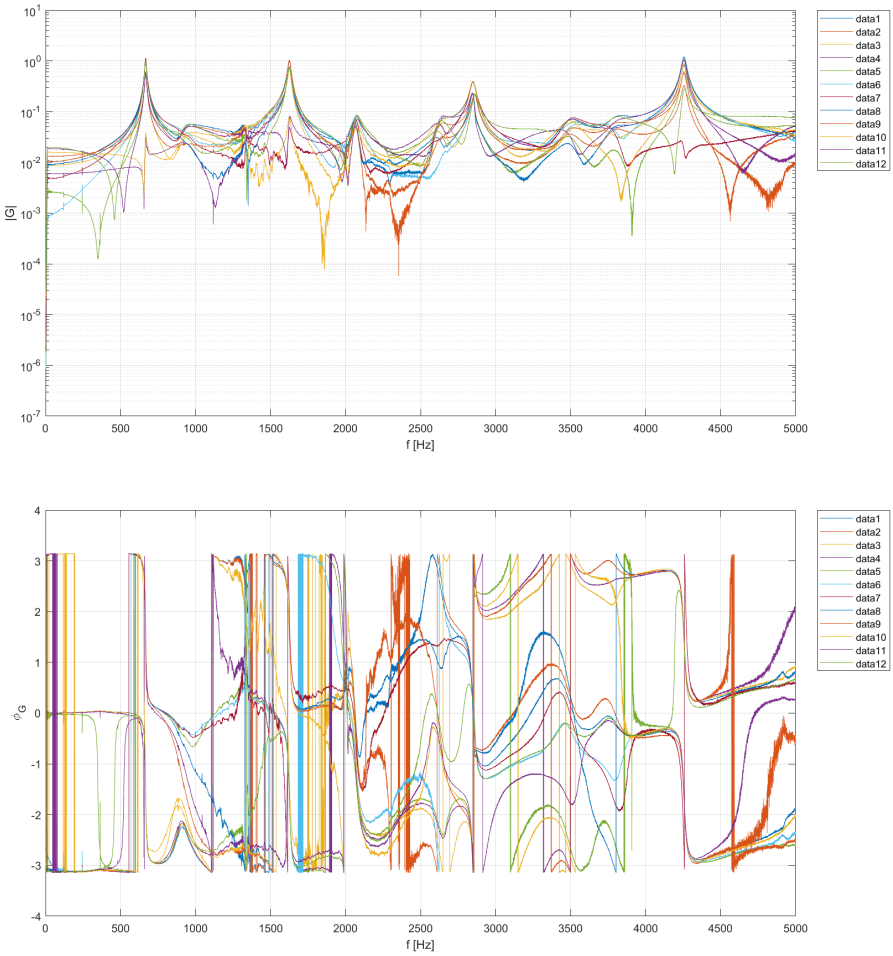

Figure 13: Modules and phases of the experimental FRFs

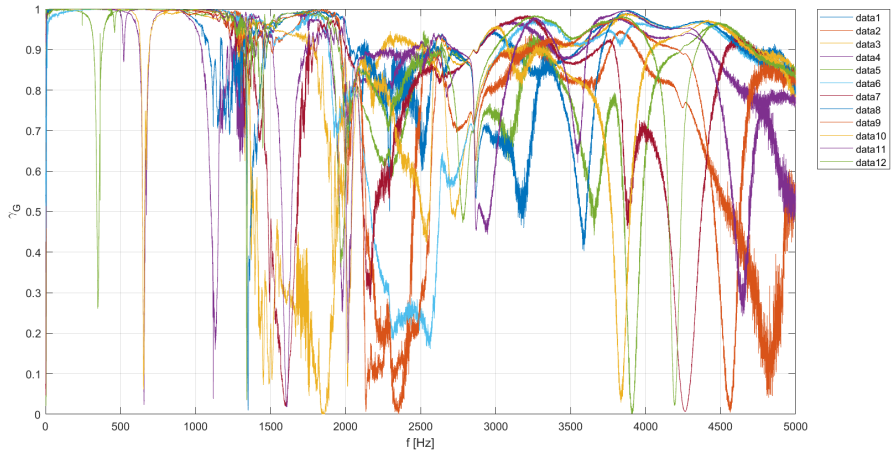

Figure 14: Coherence function

It is immediately evident that most of the FRFs display four major peaks, each corresponding to a phase shift in the phase diagram. These peaks correspond to the axial modes of the railway wheel, and their frequency positions will be used for extracting modal parameters and identifying mode shapes. Some FRFs (numbers 4 and 10 for the first mode and numbers 3, 7 and 11 for the second one), instead, exhibit an anti-resonance peak immediately followed by a resonance peak. This pattern indicates that the sensors recording these signals are positioned near a node, as detailed towards the end of section 2.2.

Examining the coherence, we observe that its value is close to one, particularly for the first two modes, except for the signals from sensors near a node in which the coherence drops almost to zero. At higher frequencies, we observe a progressive decrease in coherence, which is expected due to the nature of the impact test. Indeed, the hammer excites high-frequency components with less energy compared to low-frequency ones, resulting in an input signal with decreasing quality at higher frequencies.

Moreover, we can also see a small peak near $2100\ Hz$ which probably corresponds to the interference of a radial mode of the wheel in the measurements. This can be spotted by looking at the strange behaviour of the phase diagram (unclear phase shift).

3.3 Modal identification

The procedure extensively developed for the part A of the assignment in section 2.3 and the related code are used to identify the modal parameters (natural frequencies, adimensional damping ratios and modeshapes) of the first axial modes of the wheel of the rail vehicle.

The output of the Matlab code is shown below. The reconstruction seems successful, both for the phase and the amplitude of the FRFs (*figure 15*). Concerning the modeshapes, they are reported in *figure 16*, while the reconstructed modal parameters are shown in *table 3*.

Parameter	**Symbol**	**Reconstructed value**	**Unit**
natural frequencies	f_1	667.3	Hz
	f_2	1625.3	Hz
	f_3	2848.0	Hz
	f_4	4256.3	Hz
nondim. dampings	ξ_1	0.751	%
	ξ_2	0.554	%
	ξ_3	1.756	%
	ξ_4	0.371	%

Table 3: Reconstructed modal parameters

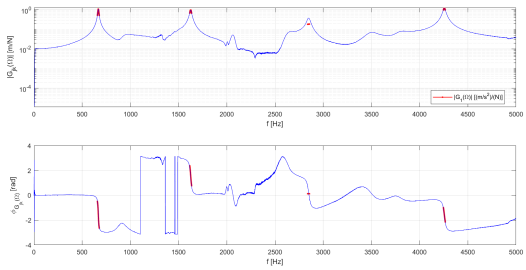

(a) Reconstruction of the FRF for sensor 1

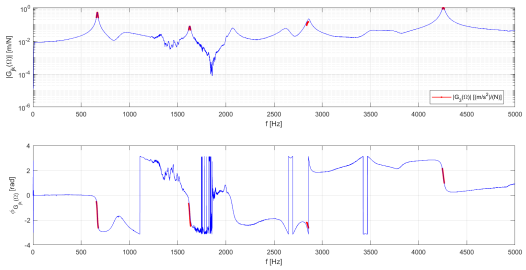

(b) Reconstruction of the FRF for sensor 3

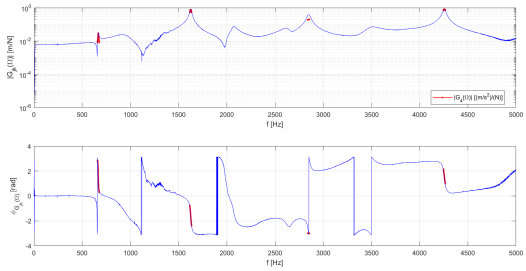

(c) Reconstruction of the FRF for sensor 4

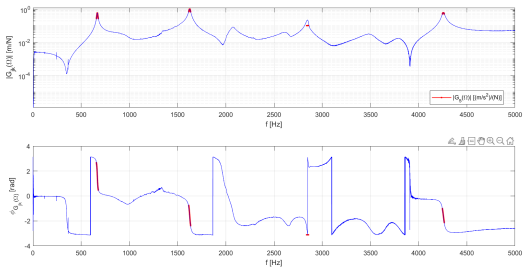

(d) Reconstruction of the FRF for sensor 5

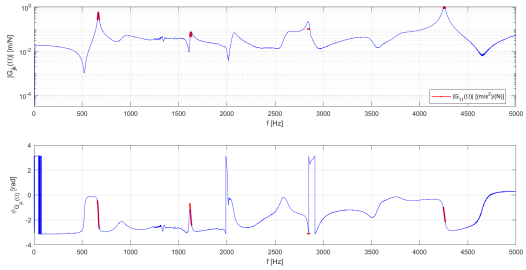

(e) Reconstruction of the FRF for sensor 11

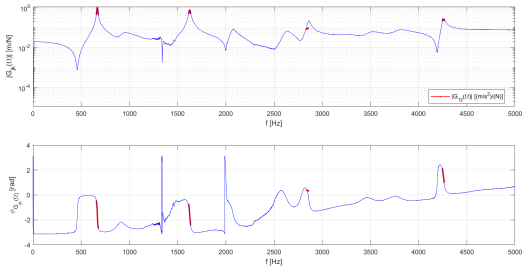

(f) Reconstruction of the FRF for sensor 12

Figure 15: Reconstruction of the FRFs

Analysis of the results The FRFs are well reconstructed especially for the first two modes. We obviously still see the antiresonance-resonance behaviour for some peaks in the FRFs related to sensors placed near a node as discussed before (e.g. sensors 4 and 11). Furthermore, an antiresonance can be found in the frequency response functions without an adjacent resonance. This should not be attributed to the force or sensor being near a node but rather to the combination of different contributions with opposite phases (e.g. sensors 5, 11 and 12).
As we can see, there are some zones in the FRFs that are scattered. This is due to the poor coherence. Moreover, we can clearly see that the third mode is badly reconstructed in all FRFs. This issue arises due to an error in the experimental setup, specifically related to the mounting of the wheels in the free-free condition using the springs. Indeed, we see in the FRF a strange shift in some of the peaks. Therefore, no relevance should be given to these components neither to the corresponding modeshapes.
The fourth modeshape is not meaningful too, as we see a progressive drop in the coherence for high frequencies.

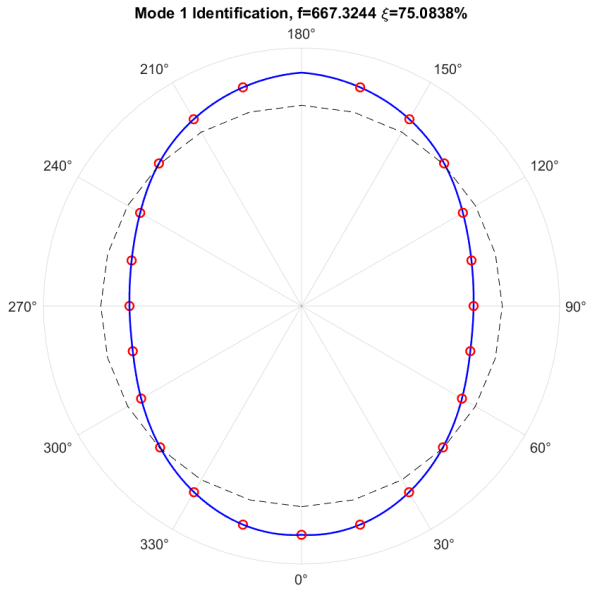

(a) Reconstruction of the first modeshape

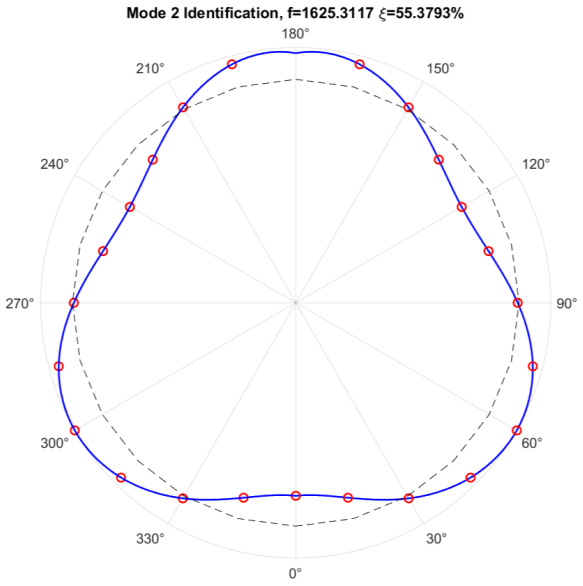

(b) Reconstruction of the second modeshape

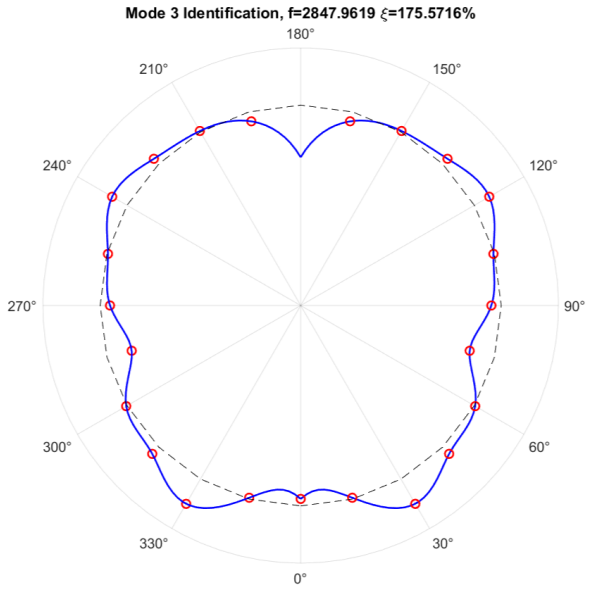

(c) Reconstruction of the third modeshape

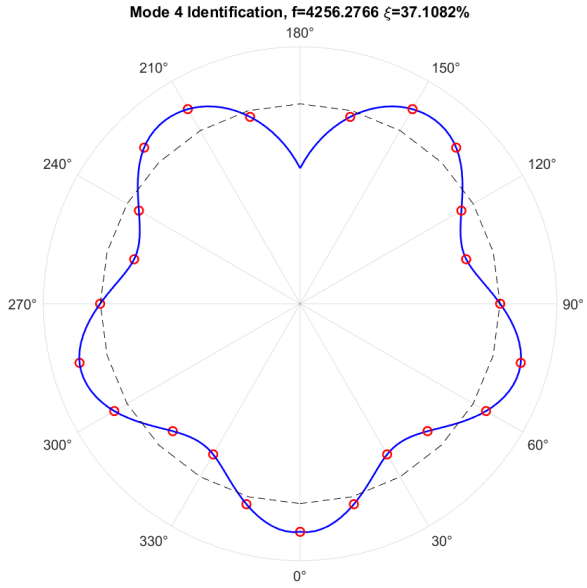

(d) Reconstruction of the fourth modeshape

Figure 16: Reconstructed modeshapes

4 Conclusions

The modal analysis we developed seems successful for both the considered structures: we were able to extract modal parameters and modeshapes through the implementation of a simple minimisation procedure, to gain information about a specific frequency range of interest (first four modes for the beam and first two modes for the wheel).
However, we realised that there are some important factors we need to pay attention to. First, we used is a single-degree-of-freedom method, meaning that the mathematical model we developed for the modal parameters optimisation

procedure is able to reconstruct one mode at the time: for this reason, as previously mentioned, this analysis is only valid if the natural frequencies of the structure are "far enough" one to the other and the behaviour of the FRF in correspondence of a resonance peak is almost exclusively described by the mode associated to it: this usually happens when the structural damping is low. Moreover, we saw that it is important to correctly set the experimental procedure, in particular paying attention to the position of the input and of the sensors. It is also important to take in account for the nature of the input force, while analysing the data: as we saw in the case of the rail wheel, for example, the impact hammer is only able to provide enough energy up to a certain frequency. Finally, we always need to account for the fact that there could be some physical phenomena that are not considered in our mathematical model of the structure, which may cause an unexpected behaviour of the results.